Timing of readiness potentials reflect a decision-making process in the human brain

Kitty K. Lui [a], Michael D. Nunez [a,b,*], Jessica M. Cassidy [c], Joachim Vandekerckhove [a,d], Steven C. Cramer [c,e], Ramesh Srinivasan [a,b]

[a] Department of Cognitive Sciences, University of California, Irvine USA
[b] Department of Biomedical Engineering, University of California, Irvine USA
[c] Department of Neurology, University of California, Irvine USA
[d] Department of Statistics, University of California, Irvine USA
[e] Department of Anatomy & Neurobiology, University of California, Irvine USA

[*] Corresponding Author: mdnunez1@uci.edu
Michael D. Nunez ORCID: 0000-0002-9965-6282

Acknowledgements

This research was supported by a grant from the NSF to JV and RS (1658303) and grants from the NIH to SC (K24HD074722, T32AR047752, and K99HD091375) and from the University of California, Irvine Institute for Clinical and Translational Science to JC (UL1-TR000153). Kiana Scambray is thanked for her help with data analysis in studies related to this paper. Jennifer Wu and Vu Le are thanked for their help on task design and construction of splint apparatus to record responses for this paper.

Abstract

Decision-making in two-alternative forced choice tasks has several underlying components including stimulus encoding, perceptual categorization, response selection, and response execution. Sequential sampling models of decision-making are based on an evidence accumulation process to a decision boundary. Animal and human studies have focused on perceptual categorization and provide evidence linking brain signals in parietal cortex to the evidence accumulation process. In this study we use a task where the dominant contribution to response time is response selection and model the response time data with the drift-diffusion model. EEG measurement during the task show that that the Readiness Potential (RP) recorded over motor areas has timing consistent with the evidence accumulation process. The duration of the RP predicts decision-making time, the duration of evidence accumulation, suggesting that the RP reflects an evidence accumulation process for response selection. Thus, evidence accumulation may be a neural implementation of decision-making processes in both perceptual and motor systems, that are estimated as a unitary process in sequential sampling models. The contributions of perceptual categorization and response selection to evidence accumulation processes in decision-making models can be potentially evaluated by behavioral data with both perceptual and motor EEG signals.

Keywords

Decision making; electroencephalography; readiness potential; motor preparation; perceptual categorization; response selection

Introduction

Decision-making has been extensively studied using two-alternative forced choice tasks that incorporate multiple stages of information processing (Ratcliff et al. 2016). In these tasks, participants typically perceive a visual or auditory stimulus (perception), categorize the stimulus and select one of two responses (decision-making), and respond with a motor action (response execution). Behavioral data consisting of response time and accuracy have been modeled by a number of sequential-sampling models (SSM) including drift-diffusion models (DDM; Link and Heath 1975; Ratcliff and McKoon 2008), linear ballistic accumulator models (Brown and Heathcote 2008) and leaky competing accumulator models (Usher and McClelland 2001), among others. In these models, sensory information is first encoded, followed by an evidence accumulation process to a threshold which triggers motor planning and execution. When fitting DDMs to behavioral data, sensory encoding time and motor execution time are typically estimated using a single parameter labeled *non-decision time*. The remaining time, labeled here as *decision-making time*, is the period of evidence accumulation, which is treated as a unitary process in all sequential sampling models.

Both animal and human researchers have found neural markers of evidence accumulation in electrophysiology by focusing on perceptual processing in the parietal cortex (see Shadlen and Kiani 2013; Kelly and O'Connell, 2013; O'Connell et al. 2018). For instance, direct recordings from parietal cortical neurons (found in the lateral intraparietal area; LIP) in monkeys have identified cells whose firing rates progressively increase prior to a decision and response (Roitman and Shadlen 2002; Huk and Shadlen 2005, Churchland et al. 2008). The changing firing rates of these neurons are consistent with the theoretical account of accumulation of evidence to a boundary that is central to decision-making in SSMs. Moreover, in these studies, as the strength of sensory signals increases, the rate of increase in firing rate is enhanced, suggesting a faster rate of information accumulation that leads to faster response times and more accurate decisions (Roitman and Shadlen 2002).

These findings in animal models have motivated studies in humans using EEG to identify a signal that ramps to a decision threshold, providing independent information about the rate and timing of decision-making (Kelly and O'Connell 2013; Philiastides et al. 2014). A number of studies have focused on the P300, a stimulus-locked evoked potential that increases its positive amplitude over parietal electrodes, reaching a maximum at least 300 ms after stimulus presentation (Philiastides et al. 2006; Ratcliff et al.

2009) or the related central-parietal positivity (CPP) to better account for the variability in the timing of the peak of positive potentials across different experiments (O'Connell et al. 2012; Kelly and O'Connell 2013; Rangelov, and Mattingley 2020). The P300 and CPP amplitudes are sensitive to stimulus probability and stimulus salience (Polich et al. 1996; Smith and Ratcliff 2004), such that low-probability and high-salience sensory events elicit higher amplitude signals. Moreover, the parietal signals have been observed for both auditory and visual stimuli, suggesting that they are supramodal responses (Polich et al. 1996; O'Connell et al. 2012) related to perceptual categorization (Duncan-Johnson and Donchin 1977; Kutas et al. 1977; Kotubuchey and Lang 2001; Azizan et al. 2006).

Both the amplitude and the timing of the CPP and P300 have been suggested as indicators of the evidence accumulation process. In a study using stimuli with different levels of salience and a categorical discrimination (face/car), the magnitude of the P300 parietal signal correlated to the drift-rate in a drift-diffusion model of the response data (Philiastides et al. 2006). In another study using vigilance tasks, the detection of gradual reductions in stimulus contrast evoked a CPP that was delayed as response time increased and peaked at the time of response execution (O'Connell et al. 2012). Critically, this signal was found across sensory modalities (auditory and visual) (Polich et al. 1996; O'Connell et al. 2012) and even in decision-making tasks not requiring a motor response (O'Connell et al. 2012). A similar effect could be observed for motion discrimination, with a delayed and smaller CPP peak amplitude as motion coherence decreased (Kelly and O'Connell 2013). This relationship has also been found for more complex perceptual tasks such as mental rotation (van Ravenzwaaij et al. 2017).

However, decision-making that requires a motor response (such as a button press) has at least two components: *perceptual categorization* and *response selection*, with these two components possibly occurring in parallel. Implicit in the design of the experiments described above is the notion that evidence accumulation in decision-making is a perceptual process leading to perceptual categorization (by crossing an evidence threshold), which triggers response execution. We propose that, depending on task demands, both perceptual categorization and response selection contribute to the time course of decision-making. This would explain, for instance, why O'Connell et al. (2012) found left-hemisphere beta (LHB) also accounts for much of the variance in response times and is affected by perturbations in evidence when a button response is required. The readiness potential (RP) recorded over motor areas has been interpreted as activity related to response selection in preparation for, and distinct from,

response execution (Eimer 1998; Alexander et al.,2016). The purpose of this this study is to determine if the RP could also reflect the evidence accumulation processes as estimated by the drift-diffusion models.

To test this idea, in this study we make use of the drift-diffusion model to model behavioral data in a two-alternative forced choice (2AFC) task known as the Action Selection (AS) task (O'Shea et al. 2007). In the AS task, the participants are presented one of four different stimuli varying along two dimensions (shape and size) and respond with one of two shoulder rotations. We make use of a drift-diffusion model to separate the additive contributions of *non-decision time* (NDT: for perceptual preprocessing and motor execution) and *decision-making time* (DT) to *response time* (RT) while participants perform the AS task. The drift-diffusion model makes use of a unitary evidence accumulation process to model decision-making time, which we hypothesize incorporates both perceptual categorization and response selection. Using EEG recordings, we show that, in the AS task, neither perceptual decision-making signals, the P300 (Philiastides et al. 2006), nor perceptual encoding signals, the N200 (Rungratsameetaweemana et al. 2018; Nunez et al. 2019a) account for variability in decision-making time while the RP recorded over the motor system has timing consistent with the drift-diffusion model estimate of decision-making time. In a control task without any decision-making, the Execution Only (EO) task, we find no relationship between the timing of the RP and response time.

Decision-making time is modeled as a unitary evidence accumulation process in the drift-diffusion model. In the AS task, it appears that response selection as encoded by the RP makes the dominant contribution to decision-making time. This close relationship suggests that the RP reflects an evidence accumulation process for response selection, and supports the notion that evidence accumulation is a general neural implementation of decision-making in both perceptual and motor systems.

Methods

Participants

Fifteen adults participated in this study. All participants met the following inclusion criteria: at least 18 years of age, right-handed, and English-speaking. Right hand dominance was verified using the

Edinburgh Handedness Inventory (Oldfield 1971). Participants were not able to participate if they demonstrated any of the following exclusionary criteria: inability to maintain attention or understand verbal instructions, any major neurological, psychiatric, or medical disease, or a coexisting diagnosis impacting arm/hand function. One participant was removed from analysis due to the EEG being contaminated pervasive muscle artifact, which made it difficult to estimate slow-wave potentials (i.e. the RP and P300), resulting in a sample size of fourteen adults (age 18-26 years; 9 female). This study was approved by the University of California, Irvine Institutional Review Board. Each subject provided written informed consent.

Procedure

Participants performed two different tasks that required evaluation of a visual stimulus and a motor response. Each sat with their back on a chair, hips and knees at approximately 90 degrees, and right forearm in a splint. Participants completed 4 blocks (40 trials per block) of the Action Selection (AS) task and 4 blocks (40 trials per block) of the Execute Only (EO) task. The blocks alternated for all participants, starting with AS task. After each block, participants received a 30 second rest break that was prompted by a black screen on the laptop (Fig. 1b).

Each block of trials began with an instruction presented for 30 seconds (Fig. 1a). On each trial (Fig. 1b), participants focused on a fixation cross. A stimulus (i.e., shape) appeared for two seconds and the response was given by the internal (inward) or external (outward) rotation of the right shoulder by 17.5 degrees using a forearm splint apparatus (Fig. 1c), until the splint made contact with a button embedded in either lateral wall. The purpose of the splint apparatus was to minimize compensatory movements by forearm and/or hand and thereby limit movement to a single direction in a single joint (i.e., right shoulder rotation). Participants could respond as soon as the stimulus is presented, and up to 3000 ms after stimulus presentation. Participants' responses were recorded when they depressed the button, indicating movement completion. The intertrial interval was randomized between 1 to 3.5 seconds. Participants received verbal instruction to move their arm to the middle of the apparatus after each trial.

Experimental Tasks

The AS task (O'Shea et al. 2007) is a two-alternative forced choice (2AFC) task. Participants were instructed to perform external right shoulder rotation (move the splint outward) when they saw either a big square or small circle, and instructed to perform internal right shoulder rotation (move the splint inward) when they saw either a big circle or small square. The large shapes spanned 2 degrees of visual angle while the small shapes spanned 1 degree of visual angle.

The EO task is a simple reaction time task which was used as a control condition which generated all of the behavioral data and evoked potentials without any decision-making. Participants were instructed to move their right forearm, via shoulder rotation, to only one side within a given block, upon stimulus onset, irrespective of the size and shape presented. The EO blocks alternated between performing only internal rotations and performing only external rotations.

Drift-Diffusion Model of Response Time

The response time (RT) and choice data for all participants and both conditions were simultaneously fit to a hierarchical drift-diffusion model (DDM), using a Bayesian estimation method with Markov Chain Monte Carlo samplers (Plummer 2003; Vandekerckhove et al. 2011; Lee and Wagenmakers 2013 Waberisch and Vandekerckhove 2014). Fitting parameters of DDMs adds to the analysis of human behavior by assuming simple underlying cognitive processes which have some empirical validation (Voss et al. 2004). DDMs also add to the cognitive interpretation of EEG and functional magnetic resonance imaging (fMRI) signals by relating cognitive parameters to observed cortical dynamics (Mulder et al. 2014; Nunez et al. 2015; Turner et al. 2015; Nunez et al. 2017; Turner et al. 2017; Nunez et al. 2019a).

In a DDM of decision-making it is assumed that humans accumulate evidence for one choice over another in a random-walk evidence-accumulation process with an infinitesimal time step until sufficient evidence is accumulated to exceed the threshold (labeled *boundary separation*) for either the correct or the incorrect choice. That is, evidence E accumulates following a Wiener process (i.e. Brownian motion) with an average rate of evidence accumulation (labeled *drift rate*) until enough evidence for a correct decision over an incorrect decision is made (see Ratcliff et al. 2016 for a further discussion). The instantaneous variance (labeled *diffusion coefficient*) was fixed at 1.0 in this study, because only two of the three evidence dimension parameters can be uniquely estimated (Ratcliff 1978;

Ross 2014; Nunez et al. 2017). The drift rate and boundary separation can always be scaled by the diffusion coefficient and produce the same fit.

Our hierarchical model was fit such that we could estimate separate model parameters for each participant. Each cognitive parameter of each participant was drawn from a single task-level population (AS or EO). This meant that we assumed that drift-diffusion cognitive parameters (drift rate δ, boundary separation α, and non-decision time τ) varied across participants (p) and the two tasks (t), but that there was similarity across the participants within each task. Adding these hierarchical parameters (mean parameters μ and standard deviation parameters σ) to summarize participants in each task yields better estimates of parameters due to shrinkage, a phenomenon whereby parameters are better estimated because hierarchical relationships enforce similarity across each parameter (Gelman et al. 2014). Task-level Bayesian priors for hierarchical drift-diffusion model parameters were wide normal distributions. The prior distributions were centered at 1 for drift rate and boundary separation with standard deviations of 2 and 0.5 respectively. These two parameters are scaled by arbitrary evidence units dependent upon the scale imposed by the choice of fixed diffusion coefficient (here fixed at 1). The prior distribution for non-decision time τ was centered at 300 ms with a standard deviation of 250 ms and truncated at 0 ms.

To refine our estimates of model parameters, we modeled the presence of contaminant trials to remove them from the decision-making model. Contaminant trials are defined as RT observations that are not due to an evidence accumulation process and are due to another random process. Because these RTs are not due to a decision process, the associated accuracy on those trials should be about 50% in a two-alternative forced choice task. DDM parameters are not well estimated in the presence of contaminant trials, so like previous implementations (Drugowitsch et al. 2012; Nunez et al. 2019) we assumed that every participant in each condition (AS or EO) had some proportion of trials that were generated with a random response (Bernoulli distribution with probability parameter equal to .5) and a random (Uniformly distributed) RT between 0 and a large RT (bounded by the maximum observed RT for that participant in that particular task). The overall hierarchical model of accuracy and RT data (vector $\boldsymbol{y}$) per trial (n) is defined by the following normal (N), truncated normal (with truncation between a and b denoted by $\in (a, b)$) , gamma (Γ), and uniform (U) hierarchical, prior, and likelihood distributions:

$$\tau_{pt} \sim N(\mu_{(\tau)t}, \sigma^2_{(\tau)}) \in (0,1) \quad ; \quad \mu_{(\tau)t} \sim N(0.3, \quad 0.25^2) \quad ; \quad \sigma_{(\tau)} \sim \Gamma(0.2, 1)$$

$$\alpha_{pt} \sim N(\mu_{(\alpha)t}, \sigma^2_{(\alpha)}) \in (0.1, 5) \; ; \; \mu_{(\alpha)t} \sim N(1, 0.5^2) \; ; \; \sigma_{(\alpha)} \sim \Gamma(1, 1)$$

$$\delta_{pt} \sim N(\mu_{(\delta)t}, \sigma^2_{(\delta)}) \; ; \; \mu_{(\delta)t} \sim N(1, 2^2) \; ; \; \sigma_{(\delta)} \sim \Gamma(1, 1)$$

$$\lambda_{pt} \sim U(0, 1)$$

$$\boldsymbol{y}_n \sim (1 - \lambda_{pt})\, DDM\,(\tau_{pt}, \alpha_{pt}, \delta_{pt}) + \lambda_{pt} U(-\max(RT), \max(RT))$$

Response time (RT) is defined as the amount of time after the stimulus onset for the participant to depress one of the two lateral wall buttons with the forearm splint apparatus. *Decision-making time (DT)* is the amount of time it takes to accumulate evidence to threshold (modeled by the random walk process), while *non-decision time (NDT)* is the amount of time not associated with evidence accumulation , such as *visual encoding time* (i.e. the amount of time that the brain takes to recognize that evidence must be accumulated after visual onset; see Nunez et al. 2019) and *motor execution time* (i.e. any time after decision-making occurs but before the response is recorded by the computer, including arm movement time in the apparatus).

For this study, the primary analysis focused on the posterior distributions of NDT for the two tasks because our hypotheses involved only the DT and NDT per participant and not the underlying shape of the DT and NDT distributions. Medians of posterior distributions of NDT were used as parameter estimates and were subtracted from response times on each trial to obtain estimates of decision-making time for each trial.

EEG Recording

The participants were fit with a 256-electrode EEG cap (HydroCel Sensor Net, Electrical Geodesics, Inc., Eugene, Oregon, USA). The cap was placed on the participant's head after 10 practice trials of the AS task were completed to familiarize them with the experimental procedures. EEG data were sampled at 1000 Hz using a high-input impedance Net Amp 300 amplifier (Electrical Geodesics, Inc.) and NetStation 4.5.3 software. The EEG signals were referenced to the vertex electrode (Cz) during recording. The inputs from the splint apparatus were recorded by the EEG amplifier, using separate channels to record respective buttons for internal and external shoulder rotation movements. The onset of the stimulus was recorded by the EEG amplifier using a light detector (Cedrus, San Pedro, California, USA) for precise timing information synchronized with the EEG.

EEG Preprocessing

All EEG analysis was performed using original MATLAB (Natick, MA) programs. The EEG data were detrended and segmented into trials starting 1000 ms prior to stimulus onset up to 2500 ms after the stimulus for a total duration of 3500 ms. Any trials where the participants either responded incorrectly (wrong rotation direction), did not respond at all, or responded either too rapidly (within 200 ms) or too slowly (more than 2.3 seconds) from the stimulus onset, was deemed an incorrect response. If participants responded more than once in one trial, the first response was considered their response. Bidirectional autoregressive interpolation was performed on each EEG channel from 5 to 30 samples after the response on each trial to remove an artifact created in the EEG by the input signal from the switches on the splint apparatus. As all data analysis took place in the interval prior to the response, this interpolation did not affect any of the results and was only performed to facilitate visualizing the results. The EEG data was high-pass filtered at 0.25 Hz (0.25 Hz pass, 0.1 Hz stop, 10 dB loss) and notch filtered at 60 Hz (pass below 59 Hz and above 61 Hz, 10 dB loss) using Butterworth filters.

The EEG data was artifact edited in two stages to remove some stereotypical artifacts generated from events such as eye movement, jaw movements, or muscle activity (Nunez et al. 2016). In the first stage, by visual inspection, trials that contained any vigorous movement and channels frequently containing EMG artifacts were removed from further data analysis. After the manual inspection, the data were re-referenced to the common-average reference. In the second stage, Independent Component Analysis (ICA) was then used to classify and remove artifacts from data that were related to eye movements, electrode pops, and environmental noise. ICA components were assessed as clearly artifact or possibly containing EEG (Nunez et al. 2016). All components not marked as artifact were kept for data analysis, and only components that clearly captured artifacts such as eye blinks, eye movements, or isolated channel pops were removed. The ICA components were then projected back into channels and the data were low-pass filtered at 50 Hz (Butterworth filter, 50 Hz pass, 60 Hz stop, 10 dB loss).

Evoked potentials

For each participant, *stimulus-locked* evoked potentials (EPs) were calculated at each channel by aligning each trial to the marker of the stimulus onset and averaging across trials and *response-locked*

evoked potentials were calculated by aligning to the marker of the button press and averaging across trials. In preliminary analyses, only a trivial difference was found in either behavior (response time and accuracy) or stimulus-locked/response-locked RPs between internal and external shoulder rotations in the low-pass filtered signals. Thus, we combined trials for the two directions of rotation to analyze the behavioral data and compute the EPs.

The stimulus-locked EPs that were analyzed were the N200, P300, and stimulus-locked readiness potentials (RPs). In order to isolate each EP component, without contributions from other EPs, the P300 and stimulus-locked RPs were low-pass filtered at 4 Hz (Butterworth filter, 4 Hz pass, 8 Hz stop, 10 dB loss). In these EPs, the results are presented from 400 ms before the stimulus to 1500 ms after the stimulus, and baseline correction was performed by subtracting the mean potential 200 to 0 ms before the stimulus onset. The N200 waveforms were low-pass filtered at 10 Hz (Butterworth filter, 10 Hz pass, 20 Hz stop, 10 dB loss) and high-pass filtered at .25 Hz (Butterworth filter, 1 Hz pass, .25 Hz Stop, 10 dB loss). These results are presented from 400 ms before the stimulus to 1500 ms after the stimulus, and baseline correction was performed by subtracting the mean potential 100 ms to 0 ms before the stimulus onset.

The only response-locked EP analyzed is the response-locked RP which was low-pass filtered at 4 Hz (Butterworth filter, 4 Hz pass, 8 Hz stop, 10 dB loss). For the response-locked RPs, the results are presented from 1200 ms before the response to 100 ms after the response, with baseline correction performed by subtracting the mean potential in the interval 1200 to 1000 ms before the response.

Evoked Potentials with Response Time Tertile Split

The RTs for each participant were divided into three equal-sized bins to separate them into different response speed conditions (i.e., fastest, middle, slowest). The stimulus-locked EPs and response-locked RPs were calculated separately by averaging trials within the tertiles. For the response-locked RPs, the time interval analyzed for the fastest and middle conditions were 1200 ms before the response and 100 ms after the response as in the overall average. A different time interval had to be chosen for the slowest condition in order to accurately estimate the onset time due to trials with response times longer than 1200 ms. The time interval analyzed was 1500 ms before the response and 100 ms after the response, and baseline correction was performed by subtracting the mean potential in the interval 1500

to 1300 ms before the response. The fastest and middle RT trials could not have had an extended window like the slowest condition as they would potentially overlap with data from the previous trial.

Timing of the Readiness Potential: RP duration and RP onset time

We characterized the timing of the RP in terms of duration of the response-locked RPs and the onset time of the stimulus-locked RPs. The response-locked RP was calculated by averaging the EEG data aligned to the response. We identified the eight channels (out of 256) that displayed the strongest negative potential prior to the motor response which is the defining characteristic of RPs. These eight channels were located close to the midline and slightly left-lateralized over motor areas of the brain (see Fig. 3). RP duration, which was calculated from response-locked RP, was defined as the interval during which the potential remained consistently negative at these channels, starting from the initial negative deflection up to the response execution. To identify this interval, the first derivative of the RP was estimated by taking the difference of the potential at each time point from the previous time point. The start of the response-locked RP was detected at the center of the first interval where the derivative remained negative for 125 ms indicating a consistent negative deflection of the evoked potential. The duration of the RP was defined as the interval from this starting point to the button press. The onset time of the RP relative to stimulus presentation was calculated from the stimulus-locked RPs at the same eight channels with the requirement that derivative must have remained negative for 100 ms to locate the onset of the negative deflection.

N200 and P300 peak latency estimate

The N200 and P300 showed greater individual difference in scalp topography as compared to the RP. In order to estimate the peak latency for each participant we first performed a singular value decomposition (SVD) on windowed filtered EP data. For the N200, we used a window from 125 to 250 ms after stimulus onset, while for the P300 we used a window from 200 to 450 ms. For one participant with an extended P300, we used a window from 200 to 500 ms. In each participant's data we verified that the largest SVD component had a scalp topography that matched the EP component and used the latency of the highest magnitude potential as the peak latency estimate.

Statistical Tests

Analysis with linear models was performed on response-locked RP durations, stimulus-locked RP onset times, P300 peak latency, N200 peak latency and RT distribution statistics. Mixed-effects ANOVA models were used to assess the effect of task with participants as a random factor. In the RT tertile analysis, task and RT tertile were fixed factors, while participants were a random factor. Statistics reported are both F statistics and associated p-values as well as the Bayes Factors (BF), which describe the amount of evidence for a model with different means relative to a model with only one mean for both tasks, or for RT tertiles (Rouder et al. 2012).

Linear regression models between RP duration or P300 peak latency and RT or decision-time (DT) with were also carried out and a conventional F-statistic on the model is presented. The amount of evidence for a model that has a non-zero regression slope over a model which has a regression slope of zero (Kass and Raftery 1995; Rouder et al. 2012) is presented as a Bayes Factor (*BF*). Adjusted R^2 is also reported and describes the fraction of variance of the dependent variable (e.g. response time median) explained by the regressor variable (timing measures of RP). Bayes Factors (*BF1*) comparing models with regression slopes equal to 1, indicating a 1-to-1 relationship, to models with unknown regression slopes were calculated by first fitting simple regression models in JAGS (Plummer 2003) with wide priors on slope parameters (normal distribution centered on 1 with a standard deviation of 3) and then using the simple Savage-Dickey Density Ratio (Dickey and Lientz 1970; Wagenmakers et al. 2010). All other statistics were generated by either JASP, an open-source graphical software package for statistical analysis (JASP Team, 2017), or MATLAB (Natick, MA).

Surface Laplacian

The surface Laplacian was applied to the response-locked RPs to improve spatial resolution of the EEG. The surface Laplacian is the second spatial derivative of the EEG along the scalp surface, and provides an estimate of the location of focal superficial cortical sources (Nunez and Srinivasan 2006). The scalp surface was modeled using the MNI-152 average head (Mazziota et al. 1995), and the surface Laplacian was calculated along a triangular mesh representing the scalp using a three-dimensional spline algorithm (Deng et al. 2012).

Results

Behavioral Data: Response Time and Accuracy

Response times for the AS task (*M* = 1031 ms, *Md* = 992 ms, *s* = 139 ms) were much longer than the EO task (*M* = 627 ms, *Md* = 594 ms, *s* = 113 ms). A mixed-effects ANOVA model was used to analyze the RTs to estimate the effect of task with participants treated as a random factor. There was a significant effect of task on RTs ($F(1,13) = 113.54$, $p = .01$), with a decisive Bayes Factor ($BF = 10^{21}$) supporting longer RTs in the AS task. Accuracy was very high for both the EO task (*M* = .99, *s* = .003) and the AS task (*M* = .97, *s* = .03). As a consequence, EEG analysis was performed using only on the trials with no presence of EEG artifact.

Drift Diffusion Model: Decision and Non-Decision Time

We modeled the RT distributions with the drift-diffusion model to separate non-decision time (NDT) for perceptual processing and motor execution from decision time (DT). The RT distribution for each participant is shown for each task in Fig. 2. The EO task was performed faster and with less variability across trials in each participant (Fig. 2, red histograms) compared to the AS task (Fig. 2, blue histograms). This result was expected since the EO task did not require time for decision-making. Posterior distributions of the NDT parameter were estimated for both tasks across participants (population level in the hierarchical model) and for each participant in each task. For each participant and task, a 95% credible interval of the NDT is presented by a shaded bar in Fig. 2. The fastest RTs in each task were good approximations of each participant's NDT. There was a wide variability in NDTs across participants but a relatively narrow 95% credible interval within each participants' data.

For the AS task, the median of the population-level posterior distribution of NDT was 377 ms with a 95% credible interval ranging from 317 ms to 438 ms. For the EO task, the median of the population-level posterior distribution of non-decision time was 288 ms with a 95% credible interval ranging from 235 ms to 338 ms. There was very small overlap (21 ms) found between the distributions for the two tasks indicating that the probability of the NDTs being the same between the AS task and the EO task was very small.

The DDM can be used to decompose RT into additive components of NDT and DT. For the AS task, median RT was 992 ms, and the NDT estimate was 377 ms, indicating typical DT of around 615 ms. In the EO task, median RT was 594 ms, and the NDT estimate was 288 ms, indicating typical DT of approximately 306 ms. Thus, the longer RTs exhibited in the AS tasks (~400 ms longer than EO) result from both longer DT (~310 ms) and longer NDT (~90 ms). However, individual differences were apparent in both decision and non-decision time as shown in Fig. 2, which we exploited to investigate the relationship between decision-making time and the readiness potential (RP) and P300.

Comparison of N200 peak latency between tasks

We examined the timing of the N200 in relation to the estimates of NDT estimates in each task obtained from the drift-diffusion model. The N200 and P300 are stimulus-locked EPs recorded over occipital and parietal electrodes. Fig. 3 (a and b) shows the waveforms and topographic maps of each evoked potential for each task averaged over all participants. The waveforms are averaged over the 8 strongest electrodes indicated in the topographic map.

The N200 shows the characteristic of negativity over occipital cortex at around 180 to 220 ms (Patel and Azzam 2005), and bilateral topography with the 8 strongest electrodes in the average over participants distributed over both hemispheres. There was minimal difference in the N200 peak latencies between the two tasks at these 8 electrodes (Fig. 3a). The AS task had a median N200 peak latency of 173 ms (M = 171. 86 ms, s = 26 ms) and the EO task had a median N200 peak latency of 168.5 ms (M = 165.29 ms, s = 26 ms). N200 peak latencies were analyzed using a mixed-effects ANOVA, with participants treated as a random factor, indicating no significant difference found between the AS task and the EO task ($F(1,13) = 3.72$, $p = .07$, with $BF = 1.16$).

NDT consists of sensory encoding and response execution. In the behavioral data, we found the AS task has ~90 ms longer NDT, while the N200 peak latency indicates no difference between tasks. Because N200 peak latencies are thought to track sensory encoding time (Nunez et al., 2019a), this suggests that the difference between tasks in non-decision time is due to response execution time. This might be expected as the AS task requires reprogramming a new response on each trial, while the EO task can be automated as the same response is required on each trial.

Comparison of P300 peak latency and RP duration between tasks

The P300 is a positive potential recorded over parietal electrodes (Patel and Azzam 2005). The P300 waveform and topographic map is shown in Fig. 3b, with the waveform averaged over the 8 strongest electrode, distributed bilaterally over both hemispheres. The median P300 latency in the AS task was 326.5 ms (M = 327.5 ms, s = 47 ms) and in the EO task was 289.5 ms (M = 294.64 ms, s = 44 ms). A mixed-effects ANOVA with participants treated as a random factor showed a significant difference between tasks; ($F(1,13) = 12.58$, $p < .01$, with $BF = 112.57$). The P300 peak latency was delayed by about 40 ms in the AS task as compared to the EO task.

We calculated the response-locked RPs for each participant to evaluate if the longer RTs in the AS task compared to EO task were reflected in the readiness potential (RP). The response-locked RP is a negative potential that begins prior to the response and reaches a negative peak at movement onset (Eimer 1998; Alexander et al. 2016). Fig. 3c shows the average across participants of the response-locked RPs, averaged across the eight channels with the strongest negative potential (selected from all channels) for both tasks. In our experiment, the button push corresponded to the completion of shoulder internal or external rotation, so the minimum preceded the response marker by around 225 ms. This had little impact on the interpretation of the results, as the movement was identical in the two tasks and the response-locked RP reached a minimum at the same time around -250 to -200 ms in each participant and task. Fig. 3c shows the EEG topographies of the averaged potentials over the time period of the minimum peak (-250 ms to -200 ms). In these data, the response-locked RP showed a strong negative potential close to the midline and slightly left-lateralized.

The duration of the response-locked RP was defined as the time interval from the initial negative deflection of the response-locked RP (i.e., when the signal showed a consistent negative ramp), to the button press indicating completion of movement. The duration of the response-locked RP for the AS task (M = 870 ms, Md = 921, s = 88 ms) was longer than the duration of response-locked RP for the EO task (M = 680 ms, Md = 645, s = 146 ms) by approximately 190 ms. Response-locked RP duration was compared between tasks using a mixed-effects ANOVA with participants as a random factor. There was a significant difference in response-locked RP duration between the AS task and the EO task; $F(13) = 18.72$, $p < .001$, with $BF = 304.24$ indicating substantial evidence to support a longer duration of the response-locked RP in the AS task.

Decision-making time (DT) is defined as the difference between response time and NDT and is the period of evidence accumulation in the drift-diffusion model. The AS task has about a 310 ms longer DT than the EO task. The P300 was delayed by about 40 ms which could account only a small portion of the difference in decision-making time. This difference may reflect the perceptual categorization in the AS task in comparison to stimulus detection in the EO task. In contrast, the duration of the RP was approximately 190 ms longer in the AS task than the EO task potentially indicating that response selection accounted for a large portion of the increase in decision-making time.

Comparison of Stimulus-locked RP to the P300

We examined the stimulus-locked RP at the same channels that showed the strongest negative potential for the response-locked RP for each participant in each task and compared it to the P300 recorded at parietal electrodes (Fig. 4). Similar to the response-locked RP, the stimulus-locked RPs showed a strong negative deflection at these electrodes. The onset of this negative potential occurred at a similar time for the AS task (M = 221 ms, Md = 214 ms, s = 42 ms) and the EO task (M = 251 ms, Md = 204 ms, s = 199 ms). A mixed-effects ANOVA for the stimulus-locked RP onset times of the negative deflection treating participants as a random factor showed no significant effect of task on onset times $F(1,13) = .58$, $p = .58$, with the Bayes Factor ($BF = 0.4$) This suggests highly ambiguous evidence regarding the difference between means. This also indicates that the response selection process indexed by the RP begins before the P300 peak, suggesting that the response selection and perceptual categorization take place in parallel in these tasks, consistent with previous studies showing covert EMG activity during decision-making (Servant et al. 2015)

The striking difference between tasks was the extended duration of the negative potential in the AS task as compared to the EO task. Both tasks showed a negative potential that reaches a peak magnitude at roughly 300 ms after stimulus onset. Fig. 4b shows topographic maps of the potentials at selected time points. For the AS task, the stimulus-locked EPs at 300 ms post-stimulus is characterized by a strong positive potential over parietal channels, and a negative potential is strongest at electrodes anterior to the eight channels with the strongest response-locked RP. This topography indicates that in this time window (about 300 ms after stimulus onset) the stimulus-locked RP incorporates the negative potential generated by the dipole sources of the P300. In contrast, 850 ms after the stimulus the topographic map indicated a strong negative potential with topographic distribution closely corresponding to the RP (see

Fig. 3c) and very small positive potential over parietal channels which have returned to nearly baseline (Fig. 4a). The EO task showed a topographic distribution at 300 ms which incorporated both the negative potential at electrodes exhibiting the strongest RP and the positive potential over parietal cortex suggesting the two processes are entirely concurrent. The positive potential at parietal electrodes had a smaller magnitude and shorter duration.

Stimulus-locked RP onset and Response-locked RP duration by Response Time Tertiles

We investigated if the RP onset (measured from stimulus-locked RP) or RP duration (measured from response-locked RP) was correlated to the RTs. For each participant, and in each task, the trials were sorted by RT and both stimulus and response-locked RPs were separately averaged for the trials in the slowest, middle, and fastest RT tertiles, as shown in Fig. 5.

For the AS task (Fig. 5a), the fastest RT tertile had the shortest RP duration (M = 754 ms, Md = 778 ms, s = 88 ms), then the middle RT tertile had longer RP duration (M = 815 ms, Md = 851 ms, s = 109 ms), and the slowest RT tertile had the longest RP duration (M = 1070 ms, Md = 1098 ms, s = 142 ms). For the EO task, the fastest (M = 621 ms, Md = 635 ms s = 146) and middle (M = 594 ms, Md = 526 ms s = 182 ms) RT tertiles had similar RP duration while the slowest RT tertile (M = 947 ms, Md = 918 ms s = 129 ms) had about a 300 ms longer RP duration. A mixed-effects ANOVA was used to estimate the effect of task and RT tertile on RP duration treating participants as a random factor. There was no significant interaction between task and the tertile split; $F(1,13) = 1.53$, $p = .24$, with $BF = 0.3$. There was a significant effect of task; $F(1,26) = 23.11$, $p < .001$, with very strong evidence for a difference in mean duration times between tasks ($BF = 121$), and a significant effect of RT tertile; $F(2,26) = 51.98$, $p < .0001$, with decisive evidence of a difference in mean duration between RT tertiles ($BF = 10^5$).

In contrast, the stimulus-locked RPs had onset times that were similar for the three RT tertiles in both tasks as shown in Fig. 5b. For the AS task, the fastest RT tertile had an average RP onset time at 213 ms (Md = 205 ms, s = 51 ms), the middle RT tertile had an average RP onset time of 217 ms (Md = 212 ms, s = 47 ms), and the slowest RT tertile had an average RP onset time at 228 ms (Md = 228 ms s = 42 ms). For the EO task, the fastest RT tertile had an average RP onset time of 209 ms (Md = 182 ms, s = 104 ms), the middle RT tertile had an average RP onset time of 221 ms (Md = 207 ms, s = 64 ms), and the slowest RT tertile had an average RP onset time of 222 ms (Md = 217 ms, s = 74 ms). The onset

times of the RP did not account for differences in the response time tertiles. A mixed-effects ANOVA was used to estimate the effect of task and RT tertile on onset times treating participants as a random factor. There was no significant effect found in tasks; $F(1,26) = .01$, $p = .91$, and substantial evidence for no effect of task ($BF = 0.23$) nor any effect for the RT tertiles; $F(2,26) = .72$, $p = .49$, and substantial evidence for no effect of RT tertile ($BF = 0.15$).

P300 peak latency by Response Time Tertiles

The analysis by RT tertiles was repeated with P300 peak latency as shown in Fig. 6. When plotting the P300 signal by RT tertiles, the fastest RT tertile ($M = 334$ ms, $Md = 333$ ms, $s = 45$ ms), the middle RT tertile ($M = 324$ ms, $Md = 325$ ms, $s = 45$ ms), and the slowest RT tertile ($M = 345$ ms, $Md = 326.5$ ms, s = 61 ms) peaked at nearly the same time in the AS task (Fig. 6). In the EO task, the fastest RT tertile ($M = 277$ ms, $Md = 286.5$ ms, $s = 33$ ms) and the middle RT tertile ($M = 292$ ms, $Md = 287$ ms, $s = 48$ ms) had similar P300 median peak latency, while the slowest RT tertile ($M = 332$ ms, $Md = 303$ ms, $s = 70$ ms) showed a 40 to 50 ms longer latency compared to the other two conditions.

A mixed-effects ANOVA was used to estimate the effect of task and RT tertile on the P300 peak latency treating participants as a random factor. There was a significant interaction between task and RT tertile; $F(2,26) = 6.3$, $p < 0.01$. Due to the interaction, a separate analysis was done for each task to examine the effect of RT tertile. In the AS task, there was no effect of RT tertile on P300 peak latency ($F(2,26) = 1.76$, $p = .19$, with $BF = .54$). However, a significant effect of RT tertile on P300 peak latency was found in the EO task ($F(2,26) = 11.22$, $p < .001$, with $BF = 90.6$). In the EO task the slowest RT tertile showed a delayed P300. The likeliest explanation for this delayed peak in the slowest RT tertile is lack of attention and arousal during those trials due to the repetitive nature of the EO task.

RP Duration as a Predictor of Response Time and Decision-Making Time

We tested if the duration of the RP was quantitatively related to response time (RT) and decision-making time (DT). A linear regression analysis was performed to determine if RP duration could predict RT for each task, using the RP duration and median RT computed for each RT tertile in each participant. For the AS task, RP duration was strongly correlated to median RT ($R^2 = .50$, $F(2,40) = 404$, $p < .0001$), with decisive evidence of non-zero slope ($BF = 10^4$). RP duration had a nearly one-to-

one relationship with RT for this task (Fig. 8a) with β = .90 (t(40) = 6.36) and with some direct evidence of a regression slope of 1 (*BF1* = 19.25). The intercept of 217 ms reflects additional time required to account for RT, possibly reflecting visual stimulus processing time, and is consistent with the onset time of the negative deflection in the stimulus-locked RP (see Fig. 5b).

Decision-making time (DT) was calculated for each trial by subtracting the non-decision time (median of the posterior distribution of non-decision time estimated by the drift-diffusion model) from the RT on each trial. Similar to the RT tertile analysis, the trials were sorted by DT and EPs were estimated for tertiles of DT to estimate RP duration. The RP durations for DT tertiles were combined across participants to estimate a regression model. In the AS task, the relationship between RP duration and median DT were fairly strong (R^2 = .55, F(2,40) = 47.9., p < .001), with $BF = 10^5$, and the RP duration also had a close one-to-one relationship to DT (Fig. 7b) with β = .86 (t(40) = 6.92) and *BF1* = 7.21.

In contrast, for the EO task, the RP duration did not perform as well as a predictor of either RT or DT. There was a weaker (but significant) correlation between RP duration and RT (R^2 = .27, F(2,40) = 17.1, p < .001), with *BF* = 60.16 (Fig. 7c) and a slope far less than one (β = .35, t(40) = 3.82 and *BF1* < 10^{-4}). There was also a weak (but significant) relationship between RP duration and DT (R^2 = .31, F(2,40) = 18.3, p < .001), with *BF* = 193.56. (Fig. 7d) and a slope far less than one (β = .31, t(40) = 4.28 and *BF1* < 10^{-4}).

P300 Peak Latency as a Predictor of Response-Time and Decision-Making Time

We tested P300 peak latency to see if it could predict RT or DT. In the AS task, the P300 peak latency had little to no correlation to the median RT tertiles (R^2 < 10^{-2}, F(2,40) < .01, p = .97, with *BF* = 0.3) as shown in Fig. 8a. There was almost no relationship between P300 peak latency and DT (R^2 < 10^{-2} F(2,40) < .001, p = .99), with *BF* = 0.3 as shown in Fig. 8b.

In the EO task, however, P300 peak latency did significantly correlate with RT (R^2 = .22, F(2,40) = 11.3, p = < .01), with *BF* = 19.73 , with a slope a little more than one (β = 1.21, t(40) = 3.35) as shown in Fig. 8c. There was a stronger relationship with DT and P300 peak amplitude, that was also significantly correlated (R^2 =.31, F(2,40) = 17.8, p < .001, with *BF* = 165.02. There was a slope of slightly more than 1 (β = 1.19, t(40) = 4.22) as shown in Fig. 8d. As noted earlier, in the EO task the

slowest tertile of RT was associated with a delayed P300, which likely was an effect of arousal rather than decision-making.

Surface Laplacian analysis of the RP

The RPs in each participant were processed with a surface Laplacian to identify superficial focal current sources. In both tasks, with the application of a surface Laplacian, the current density estimates were localized over the midline somewhat anterior to bilateral motor cortex. Three electrodes were positioned over the strongest signals, and the time course shows that of these three, one electrode over the right midline area showed a positive signal while two electrodes over the left midline area showed a negative signal in both tasks (Fig. 9a). This suggests that the RP involves a lateralization of current density in areas of the motor system that generate the RP. Fig. 9b shows the topographies of the surface Laplacian averaged over -250 ms to -200 ms before the response, and the three electrodes with the highest magnitude current density are marked in green, red, and blue and labeled 1-3, corresponding to the waveforms in Fig. 9a. The overall pattern shows that the right hemisphere exhibited more positive current density in comparison to the left hemisphere, for both of these tasks involving right arm movement.

Data and code availability

Artifact-correct EEG data is available upon request to the corresponding author: mdnunez1@uci.edu MATLAB and JAGS analysis code are available on https://osf.io/7r6af/ and in the following repository https://github.com/mdnunez/RPDecision (as of July 2020).

Discussion

Evidence accumulation is believed to be the underlying mechanism of decision-making, determining the time it takes to select between alternative decisions (Link and Heath 1975; Ratcliff and McKoon 2008). Previous studies have shown parietal cortex activity that exhibits characteristics of evidence accumulation, and whose time is related to response time (Shadlen and Kiani 2013; Kelly and O'Connell, 2013; O'Connell et al. 2018). In this study, the Action Selection (AS) task (O'Shea et al.

2007) was used to investigate decision-making. Response time (RT) and accuracy data was fit to a drift-diffusion model (Ratcliff and McKoon 2008) in order to partition RT into non-decision time (for stimulus encoding and motor execution) and decision-making time (corresponding to the duration of evidence accumulation). We found that the duration of the readiness potential (RP) recorded over motor-related areas of the brain has a one-to-one relationship with decision-making time. The results indicate that response selection can be modeled with an evidence accumulation process reflected in the RP.

Readiness Potential reflects decision-making in the Action Selection task

Our main objective in this study was to identify EEG signals whose timing shifted in a manner consistent with the longer decision-making time in the AS task as compared to the Execution Only (EO) task. We expected that the variability in the RTs between the two tasks would be largely due to decision-making in the AS task. Participants exhibited response times approximately 400 ms longer in the AS task than the EO task that was accounted for in the drift-diffusion model by both longer decision-making time (~310 ms) and longer non-decision time (~90 ms).

RPs display the characteristic of slow ramping negativity reaching a minimum at the start of movement, resolving to baseline as the movement completed (Eimer 1998; Alexander et al. 2016). The duration of the RPs (absolute value of the RP onset time) from the AS task was on average about 190 ms longer than the duration of the RP from the EO task. The stimulus-locked RPs at the same channels exhibited a negative ramp that onset identically at around 200 ms for both tasks indicating that the onset of the readiness potential takes place after visual encoding but before decision-making. Past work showed that variation in stimulus intensity did not affect RP duration (Miller et al. 1999), indicating that that RP is independent of perceptual processing. This suggests that the longer RPs in the AS task reflected longer decision-making time related to response selection.

To clarify if RP quantitatively tracked decision-make time, a linear regression analysis was performed with the tertile split of trials by RTs and decision-making times (DTs). In the AS task, RP duration and RT had a strong relationship with a slope close to 1 (.9), indicating a nearly one-to-one relationship between increasing duration of RP and RT (Fig. 6a). The intercept in this model was 217 ms which was consistent with time for perceptual processing (Thorpe et al. 1996; Nunez et al. 2019a), and with the

onset of the RP identified in the stimulus-locked EPs at about 200 ms. RP duration and DT also had a strong regression model (Fig. 6b) also with a slope close to 1 (.86), indicating a one-to-one relationship between RP duration and DT. These models provide strong evidence that RP duration tracks decision-making time, and that the intercepts of the regression model with RT accounted for the visual encoding time prior to the onset of evidence accumulation consistent with the onset time of the stimulus-locked RP.

In the EO task, RP duration did not predict DT and RT as well as it did in the AS task. A lack of variability in the EO task RTs, compared to AS task RTs, may partially explain this finding, as shown in Fig. 2. Moreover, in the EO task, the decision of which action to execute is fixed. As a consequence, variability in response time or decision-making time may be more strongly influenced by variability due to stimulus processing (detection) or response execution rather than in decision-making.

The P300 does not track decision-making in the Action Selection task

In previous studies, the central-parietal positivity (CPP) amplitude and timing of peak positive potential have been found to be reflective of evidence accumulation process towards a decision, and this CPP is thought to be analogous to the P300 (O'Connell et al. 2012; Kelly and O'Connell 2013). In vigilance tasks (specifically gradual reduction in contrast and motion detection task with different coherence levels), the peak of CPP was delayed as RT increased (O'Connell et al. 2012; Kelly and O'Connell 2013). As the difficulty of identifying and processing the stimulus increased, there was a delay in the CPP, with a peak right before motor execution. This was attributed to longer decision-making since the peak of the CPP occurred at motor execution. However, some of this delay may also reflect increased time for perceptual processing, as these studies employed stimuli at varying stimulus-to-noise ratios.

The task we have used in this study employed simple shapes presented without any noise, and the decision-making involves a significant component of response selection rather than perceptual categorization. The P300 was identified in each task, but the time of the peak was delayed by about 40 ms in the AS task, despite a nearly 400 ms difference in RTs (Fig. 4c) and a nearly 310 ms difference in DTs. Moreover, when the data were split into tertiles of fastest, middle, and slowest RTs, the P300 peak latency did not predict RTs or DTs. We also did not find a separate CPP from the P300 that predict RT or DT that better matched the CPP as found in other studies (O'Connell et al. 2012; Kelly

and O'Connell 2013; Rangelov, and Mattingley 2020). This could be due to different task structure and demands.

Evidence accumulators in the human brain

Decision-making includes both perceptual categorization and response selection. The CPP or P300 may reflect an evidence accumulation process for perceptual categorization. In the AS task, perceptual categorization was not decisive in determining response time. Perceptual processing is simple, and the decision-making has a large component of response selection. Our findings indicate that the RP reflects evidence accumulation in the motor system for response selection, which is decisive in determining response time in this task. Our results suggest that by monitoring both perceptual and motor signals, EEG data can be used to understand the distinct contributions of perceptual and motor decision-making to response time data depending upon the task demands.

RT and choice behavior during visual decision-making tasks are well characterized by models that assume a continuous stochastic accumulation of evidence (Link and Heath 1975; Usher and McClelland 2001; Ratcliff and McKoon 2008; Brown and Heathcote 2008; Ratcliff et al. 2016). Studies in animal models showing increasing firing rates in parietal cortex during perceptual decision-making (Roitman and Shadlen 2002; Huk and Shadlen 2005, Churchland et al. 2008), motivated the earlier studies of the P300 in parietal cortex (Philiastides et al. 2006; Ratcliff et al. 2009; O'Connell et al. 2012; Kelly and O'Connell 2013) and the present study of the RP over motor-related areas of the brain. However, the relationship between progressively increasing firing rate and ramps in slow-wave EEG potentials are complicated by a number of factors. EEG potentials reflect synchronous synaptic potentials at a macroscopic (cm) scale (Nunez and Srinivasan 2006). The sources of the EEG are the currents in extracellular space - Excitatory postsynaptic potentials (EPSPs) generate positive sources inside the membrane and negative current in the extracellular space while inhibitory postsynaptic potentials (IPSPs) generate negative sources inside the membrane and positive current in extracellular space. Thus, increasing firing rates might be expected to generate increased negative potentials as negative extracellular potentials reflect (locally) more EPSPs, suggesting that a negative ramp is related to increased cortical excitability facilitating firing of action potentials. However, we are cautious about this interpretation of the RP because of the physics of EEG recording. Scalp potentials are recorded at a distance from the cortex, and thus dominated by dipole components of the brain current source

distribution (Nunez and Srinivasan 2006; Nunez et al. 2019b). Thus, the sign of the observed potential may merely reflect whether the negative or positive pole of the dipole is closer to the scalp. Despite this complication, it is reasonable to interpret a slow ramp in EEG potentials (of either sign) as a correlate of progressive change in firing rates, providing a means to investigate accumulator processes in the human brain.

The RP duration EO task was somewhat surprising because if it were an evidence accumulator, we would not expect it to be longer than RTs. Furthermore, the only case where waveforms begin before stimulus onset is the RP estimate for the EO task. There are two possible sources of these effects. One is the application of a low pass filter at 4 Hz which smooths the onset. Another contributing cause is the automatic nature of the task. In the studies by Libet and colleagues (Libet et al. 1983) it has been suggested that response selection, indexed by the RP, precedes the conscious decision to move. In the EO task, despite the introduction of random onset times, there is essentially a repetitive motion that the subject may prepare for prior to stimulus presentation.

Sources of the Readiness Potential

The scalp topographies of the RP reveal that the strongest negative potentials occur over motor areas close to the midline and anterior to C3/C4 (Fig. 3b). The Bereitschaftspotential (BP) for finger movements is composed of an early shallow ramp over midline areas, such as supplementary motor areas (SMA) and pre-SMA and a steeper negative slope over contralateral motor areas (corresponding to C3/C4) that reaches a negative minimum at movement onset (Libet et al. 1983; Shibasaki and Hallett 2006). In our task, which involved shoulder internal and external rotation movements, the RP had a focus entirely over midline areas from RP onset to movement onset, consistent with activity in the shoulder representation in primary motor cortex which is located close to the midline (Penfield and Rasmussen 1950). The higher spatial resolution of the surface Laplacian (Fig. 7) clearly indicated a focal source close to the midline, with opposite polarities between hemispheres.

Conclusion

Decision-making has several underlying components including stimulus encoding, perceptual categorization, response selection, and response execution. In this study, we made use of a task where

decision-making mostly involved response selection. In this scenario, we find that the duration of a signal linked to the motor system, the RP, has a one-to-one relationship with amount of time required to make the decision, which is modeled by a stochastic evidence accumulation process. This close relationship between the RP and the evidence accumulation process supports the notion that an accumulator process is a general neural implementation of decision-making in both sensory and motor systems, both when individuals take actions in response to stimuli (Shadlen and Kiani 2013) or of their own free will (Schurger et al. 2012). Our results suggest that the contributions of sensory or motor systems to variability in decision-making time can be assessed by the timing of sensory and motor evoked potentials.

References

Alexander, P., Schlegel, A., Sinnott-Armstrong, W., Roskies, A. L., Wheatley, T., & Tse, P. U. (2016). Readiness potentials driven by non-motoric processes. *Consciousness and Cognition*, *39*, 38–47. https://doi.org/10.1016/j.concog.2015.11.011

Azizian, A., Freitas, A. L., Watson, T. D., & Squires, N. K. (2006). Electrophysiological correlates of categorization: P300 amplitude as index of target similarity. *Biological Psychology*, *71*(3), 278–288. https://doi.org/10.1016/j.biopsycho.2005.05.002

Brown, S. D., & Heathcote, A. (2008). The simplest complete model of choice response time: Linear ballistic accumulation. *Cognitive Psychology*, *57*(3), 153–178. https://doi.org/10.1016/j.cogpsych.2007.12.002

Churchland, A. K., Kiani, R., & Shadlen, M. N. (2008). Decision-making with multiple alternatives. *Nature Neuroscience*, *11*(6), 693–702. https://doi.org/10.1038/nn.2123

Deng, S., Winter, W., Thorpe, S., & Srinivasan, R. (2012). Improved surface laplacian estimates of cortical potential using realistic models of head geometry. *IEEE Transactions on Biomedical Engineering*, *59*(11), 2979–2985. https://doi.org/10.1109/TBME.2012.2183638

Dickey, J. M., & Lientz, B. P. (1970). The Weighted Likelihood Ratio, Sharp Hypotheses about Chances, the Order of a Markov Chain. *The Annals of Mathematical Statistics*, *41*(1), 214–226. https://doi.org/10.1214/AOMS/1177697203

Dirk, J., Kratzsch, G. K., Prindle, J. P., Kröhne, U., Goldhammer, F., & Schmiedek, F. (2017). Paper-Based Assessment of the Effects of Aging on Response Time: A Diffusion Model Analysis. *Journal of Intelligence*, *5*(2), 12. https://doi.org/10.3390/jintelligence5020012

Drugowitsch, J., Moreno-Bote, R. N., Churchland, A. K., Shadlen, M. N., & Pouget, A. (2012). The cost of accumulating evidence in perceptual decision making. *Journal of Neuroscience*, *32*(11), 3612–3628. https://doi.org/10.1523/JNEUROSCI.4010-11.2012

Duncan-Johnson, C. C., & Donchin, E. (1977). On Quantifying Surprise: The Variation of Event-Related Potentials With Subjective Probability. *Psychophysiology*, *14*(5), 456–467. https://doi.org/10.1111/j.1469-8986.1977.tb01312.x

Eimer, M. (1998). The lateralized readiness potential as an on-line measure of central response activation processes. *Behavior Research Methods, Instruments, and Computers*, *30*(1), 146–156. https://doi.org/10.3758/BF03209424

Gelman, A., Carlin, J. B., Stern, H. S., Dunson, D. B., Vehtari, A., & Rubin, D.B. (2014). *Bayesian data analysis.* 3rd Edition. Chapmna and Hall/CRC.

Huk, A. C., & Shadlen, M. N. (2005). Neural activity in macaque parietal cortex reflects temporal integration of visual motion signals during perceptual decision making. *Journal of Neuroscience*, *25*(45), 10420–10436. https://doi.org/10.1523/JNEUROSCI.4684-04.2005

Kass, R. E., & Raftery, A. E. (1995). Bayes factors. *Journal of the American Statistical Association*, *90*(430), 773–795. https://doi.org/10.1080/01621459.1995.10476572

Kelly, S. P., & O'Connell, R. G. (2013). Internal and external influences on the rate of sensory evidence accumulation in the human brain. *Journal of Neuroscience*, *33*(50), 19434–19441. https://doi.org/10.1523/JNEUROSCI.3355-13.2013

Kim, J. N., & Shadlen, M. N. (1999). Neural correlates of a decision in the dorsolateral prefrontal cortex of the macaque. *Nature Neuroscience*, *2*(2), 176–185. https://doi.org/10.1038/5739

Kotchoubey, B., & Lang, S. (2001). Event-related potentials in an auditory semantic oddball task in humans. *Neuroscience Letters*, *310*(2–3), 93–96. https://doi.org/10.1016/S0304-3940(01)02057-2

Kutas, M., Mccarthy, G., & Donchin, E. (1977). Augmenting mental chronometry: The p300 as a measure of stimulus evaluation time. *Science*, *197*(4305), 792–795. https://doi.org/10.1126/science.887923

Lee, M. D., & Wagenmakers, E.- J. (2013). *Bayesian cognitive modeling: A practical course*. Cambridge University Press. https://doi.org/10.1017/CBO9781139087759

Libet, B., Gleason, C. A., Wright, E. W., & Pearl, D. K. (1983). *Time of conscious intention to act in relation to onset of cerebral activity (readiness-potential). The* unconscious of a freely voluntary act. *Brain*, 106, 623-42. https://doi.org/10.1093/brain/106.3.623

Link, S. W., & Heath, R. A. (1975). A sequential theory of psychological discrimination. *Psychometrika*, *40*(1), 77–105. https://doi.org/10.1007/BF02291481

Mazziotta, J. C., Toga, A. W., Evans, A., Fox, P., & Lancaster, J. (1995). A probabilistic atlas of the human brain: Theory and rationale for its development. *NeuroImage*, *2*(2), 89–101. https://doi.org/10.1006/nimg.1995.1012

Miller, J., Ulrich, R., & Rinkenauer, G. (1999). Effects of stimulus intensity on the lateralized readiness potential. *Journal of Experimental Psychology: Human Perception and Performance*, *25*(5), 1454–1471. https://doi.org/10.1037/0096-1523.25.5.1454

Mulder, M. J., van Maanen, L., & Forstmann, B. U. (2014). Perceptual decision neurosciences - a model-based review. *Neuroscience*. (277), 872-884. https://doi.org/10.1016/j.neuroscience.2014.07.031

Nunez, M. D., Gosai, A., Vandekerckhove, J., & Srinivasan, R. (2019). The latency of a visual evoked potential tracks the onset of decision making. *NeuroImage*, *197*, 93–108. https://doi.org/10.1016/j.neuroimage.2019.04.052

Nunez, M. D., Nunez, P L, & Srinivasan, R. (2016). Electroencephalography (EEG): neurophysics, experimental methods, and signal processing. In Ombao, H., Linquist, M., Thompson, W. & Aston, J. (Eds), *Handbook of Neuroimaging Data Analysis* (pp. 175-197), Chapman & Hall/CRC. https://doi.org/10.13140/rg.2.2.12706.63687

Nunez, M. D., Srinivasan, R., & Vandekerckhove, J. (2015). Individual differences in attention influence perceptual decision making. *Frontiers in Psychology*, *6*, 1–13. https://doi.org/10.3389/fpsyg.2015.00018

Nunez, M. D., Vandekerckhove, J., & Srinivasan, R. (2017). How attention influences perceptual decision making: Single-trial EEG correlates of drift-diffusion model parameters. *Journal of Mathematical Psychology*, *76*, 117–130. https://doi.org/10.1016/j.jmp.2016.03.003

Nunez, P L, & Srinivasan, R. (2016). Electroencephalography (EEG): neurophysics, experimental methods, and signal processing. https://doi.org/10.13140/rg.2.2.12706.63687

Nunez, P. L., Nunez, M. D., & Srinivasan, R. (2019). Multi-Scale Neural Sources of EEG: Genuine, Equivalent, and Representative. A Tutorial Review. *Brain Topography*. *32*, 193-214 https://doi.org/10.1007/s10548-019-00701-3

Nunez, Paul L., & Srinivasan, R. (2006). *Electric Fields of the Brain: The neurophysics of EEG, 2nd ed*., New York: Oxford University Press https://doi.org/10.1093/acprof:oso/9780195050387.001.0001

O'Connell, R. G., Dockree, P. M., & Kelly, S. P. (2012). A supramodal accumulation-to-bound signal that determines perceptual decisions in humans. *Nature Neuroscience*, *15*(12), 1729–1735. https://doi.org/10.1038/nn.3248

O'Connell, R. G., Shadlen, M. N., Wong-Lin, K. F., & Kelly, S. P. (2018). Bridging Neural and Computational Viewpoints on Perceptual Decision-Making. *Trends in Neurosciences*, *14*(11), 838-852. https://doi.org/10.1016/j.tins.2018.06.005

O'Shea, J., Johansen-Berg, H., Trief, D., Göbel, S., & Rushworth, M. F. S. (2007). Functionally Specific Reorganization in Human Premotor Cortex. *Neuron*, *54*(3), 479–490. https://doi.org/10.1016/j.neuron.2007.04.021

Oldfield, R. C. (1971). The assessment and analysis of handedness: The Edinburgh inventory. *Neuropsychologia*, *9*(1), 97–113. https://doi.org/10.1016/0028-3932(71)90067-4

Patel, S. H., & Azzam, P. N. (2005). Characterization of N200 and P300: Selected studies of the Event-

Related Potential. *International Journal of Medical Sciences*. *2*(4), 147-154. https://doi.org/10.7150/ijms.2.147

Penfield, W. N., & Rasmussen, T.(1950). *The cerebral cortex of man.* New York: The Macmillan Company. https://doi.org/10.1002/ajpa.1330110318

Philiastides, M. G., Heekeren, H. R., & Sajda, P. (2014). Human scalp potentials reflect a mixture of decision- related signals during perceptual choices. *Journal of Neuroscience*, *34*(50), 16877–16889. https://doi.org/10.1523/JNEUROSCI.3012-14.2014

Philiastides, M. G., Ratcliff, R., & Sajda, P. (2006). Neural representation of task difficulty and decision making during perceptual categorization: A timing diagram. *Journal of Neuroscience*, *26*(35), 8965–8975. https://doi.org/10.1523/JNEUROSCI.1655-06.2006

Plummer, M. (2003). JAGS: A Program for Analysis of Bayesian Graphical Models Using Gibbs Sampling. In, *Proceedings of the 3rd international workshop on distributed statistical computing DSC*. (Vienna, Austria. ISSN 1609-395X)

Polich, J., Ellerson, P. C., & Cohen, J. (1996). P300, stimulus intensity, modality, and probability. *International Journal of Psychophysiology*, *23*(1–2), 55–62. https://doi.org/10.1016/0167-8760(96)00028-1

Rangelov, D., & Mattingley, J. B. (2020). Evidence accumulation during perceptual decision-making is sensitive to the dynamics of attentional selection. *NeuroImage*, 117093. https://doi.org/10.1016/j.neuroimage.2020.117093

Ratcliff, R. (1978). A theory of memory retrieval. *Psychological Review*, *85*(2), 59–108. https://doi.org/10.1037/0033-295X.85.2.59

Ratcliff, R., & McKoon, G. (2008). The diffusion decision model: Theory and data for two-choice decision tasks. *Neural Computation*, *20*(4), 873–922. https://doi.org/10.1162/neco.2008.12-06-420

Ratcliff, R., Philiastides, M. G., & Sajda, P. (2009). Quality of evidence for perceptual decision making is indexed by trial-to-trial variability of the EEG. *Proceedings of the National Academy of Sciences of the United States of America*, *106*(16), 6539–6544. https://doi.org/10.1073/pnas.0812589106

Ratcliff, R., Smith, P. L., Brown, S. D., & McKoon, G. (2016). Diffusion Decision Model: Current Issues and History. *Trends in Cognitive Sciences*, *20*(4), 260 https://doi.org/10.1016/j.tics.2016.01.007

Roitman, J. D., & Shadlen, M. N. (2002). Response of neurons in the lateral intraparietal area during a combined visual discrimination reaction time task. *Journal of Neuroscience*, *22*(21), 9475–9489. https://doi.org/10.1523/jneurosci.22-21-09475.2002

Ross, S. M. (2014). *Introduction to Probability Models*. Academic Press.

Rouder, J. N., Morey, R. D., Speckman, P. L., & Province, J. M. (2012). Default Bayes factors for ANOVA designs. *Journal of Mathematical Psychology*, *56*(5), 356–374. https://doi.org/10.1016/j.jmp.2012.08.001

Rungratsameetaweemana, N., Itthipuripat, S., Salazar, A., & Serences, J. T. (2018). Expectations do not alter early sensory processing during perceptual decision-making. *Journal of Neuroscience*, *38*(24), 5632–5648. https://doi.org/10.1523/JNEUROSCI.3638-17.2018

Schall, J. D. (2003). Neural correlates of decision processes: Neural and mental chronometry. *Current Opinion in Neurobiology*. https://doi.org/10.1016/S0959-4388(03)00039-4

Servant, M., White, C., Montagnini, A., & Burle, B. (2015). Using covert response activation to test latent assumptions of formal decision-making models in humans. *Journal of Neuroscience*, *35*(28), 10371–10385. https://doi.org/10.1523/JNEUROSCI.0078-15.2015

Shadlen, M. N., & Kiani, R. (2013). Decision making as a window on cognition. *Neuron*, *80*(2), 791-806. https://doi.org/10.1016/j.neuron.2013.10.047

Shibasaki, H., & Hallett, M. (2006). What is the Bereitschaftspotential? *Clinical Neurophysiology*, 117(11), 2341-2356. https://doi.org/10.1016/j.clinph.2006.04.025

Smith, P. L., & Ratcliff, R. (2004). Psychology and neurobiology of simple decisions. *Trends in Neurosciences*. https://doi.org/10.1016/j.tins.2004.01.006

Thorpe, S., Fize, D., & Marlot, C. (1996). Speed of processing in the human visual system. *Nature*, *381*(6582), 520–522. https://doi.org/10.1038/381520a0

Turner, B. M., Forstmann, B. U., Love, B. C., Palmeri, T. J., & Van Maanen, L. (2017). Approaches to analysis in model-based cognitive neuroscience. *Journal of Mathematical Psychology*, *76*, 65–79. https://doi.org/10.1016/j.jmp.2016.01.001

Turner, B. M., Van Maanen, L., & Forstmann, B. U. (2015). Informing cognitive abstractions through neuroimaging: The neural drift diffusion model. *Psychological Review*, *122*(2), 312–336. https://doi.org/10.1037/a0038894

Usher, M., & McClelland, J. L. (2001). The time course of perceptual choice: The leaky, competing accumulator model. *Psychological Review*, *108*(3), 550–592. https://doi.org/10.1037/0033-295X.108.3.550

van Ravenzwaaij, D., Provost, A., & Brown, S. D. (2017). A confirmatory approach for integrating neural and behavioral data into a single model. *Journal of Mathematical Psychology*, *76*, 131–141. https://doi.org/10.1016/j.jmp.2016.04.005

Vandekerckhove, J., Tuerlinckx, F., & Lee, M. D. (2011). Hierarchical Diffusion Models for Two-Choice Response Times. *Psychological Methods*, *16*(1), 44–62. https://doi.org/10.1037/a0021765

Voss, A., Rothermund, K., & Voss, J. (2004). Interpreting the parameters of the diffusion model: An empirical validation. *Memory and Cognition*, *32*(7), 1206–1220. https://doi.org/10.3758/BF03196893

Wabersich, D., & Vandekerckhove, J. (2014). Extending JAGS: A tutorial on adding custom distributions to JAGS (with a diffusion model example). *Behavior Research Methods*, *46*(1), 15–28. https://doi.org/10.3758/s13428-013-0369-3

Wagenmakers, E.-J., Lodewyckx, T., Kuriyal, H., & Grasman, R. (2010). B4ayesian hypothesis testing for psychologists: A tutorial on the Savage-Dickey method. https://doi.org/10.1016/j.cogpsych.2009.12.001

Figures

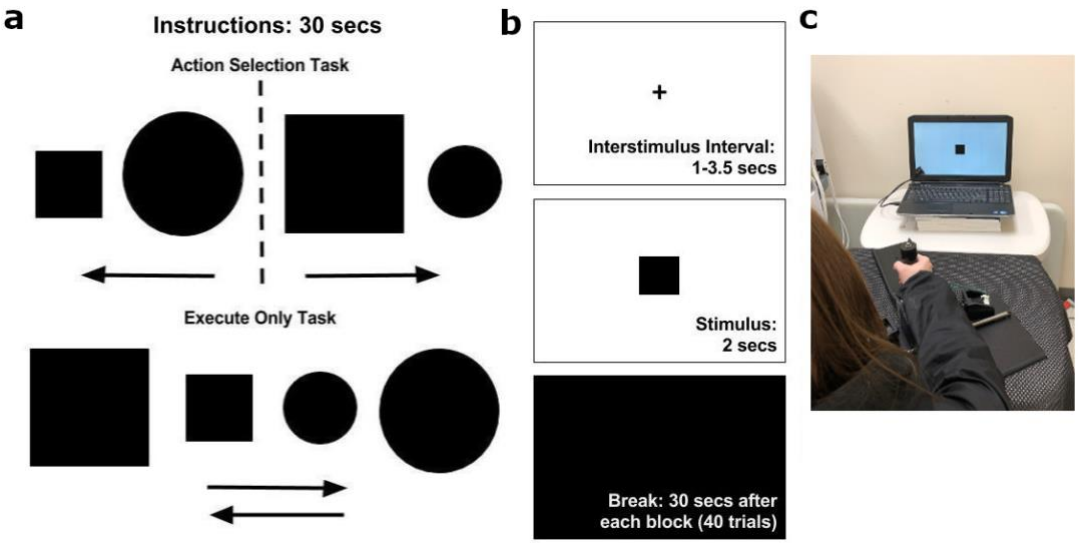

Fig. 1: a) Participants received instructions prior to each block of 40 trials. The Action Selection (AS) task instructions directed the participants to make an external rotation movement when a large square or small circle appeared, and an internal rotation movement when a large circle or small square appeared. For each Execution Only (EO) block, instructions directed participants to perform either an external rotation movement or an internal rotation irrespective of the stimulus. b) The time course of each trial. The participants fixated on a cross during an interstimulus interval of random duration ranging from 1 to 3.5 seconds. A single stimulus was presented for two seconds during which responses were collected. After each block of 40 trials, participants received a 30 second break. c) The participants used the lower arm splint apparatus to make an internal (left) or external (right) rotation of 17.5 degrees to press a switch that captured their response. The splint was used to minimize any forearm or hand movements.

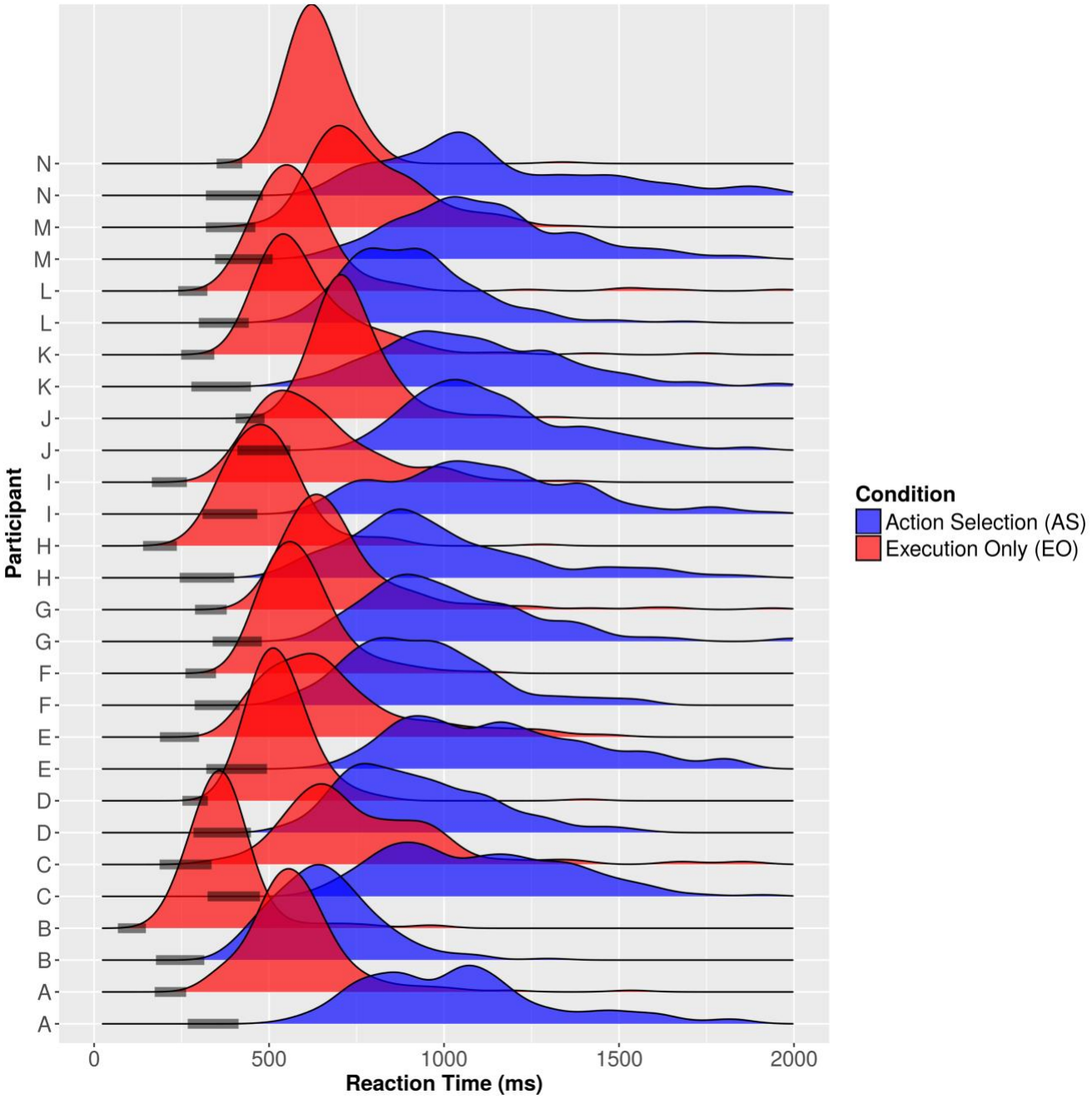

Fig. 2: Response time distributions and estimated non-decision times for each participant. Each participant had a distribution of response times for both the AS and EO tasks. 95% credible intervals of non-decision time are given by the shaded bars on the response time axis.

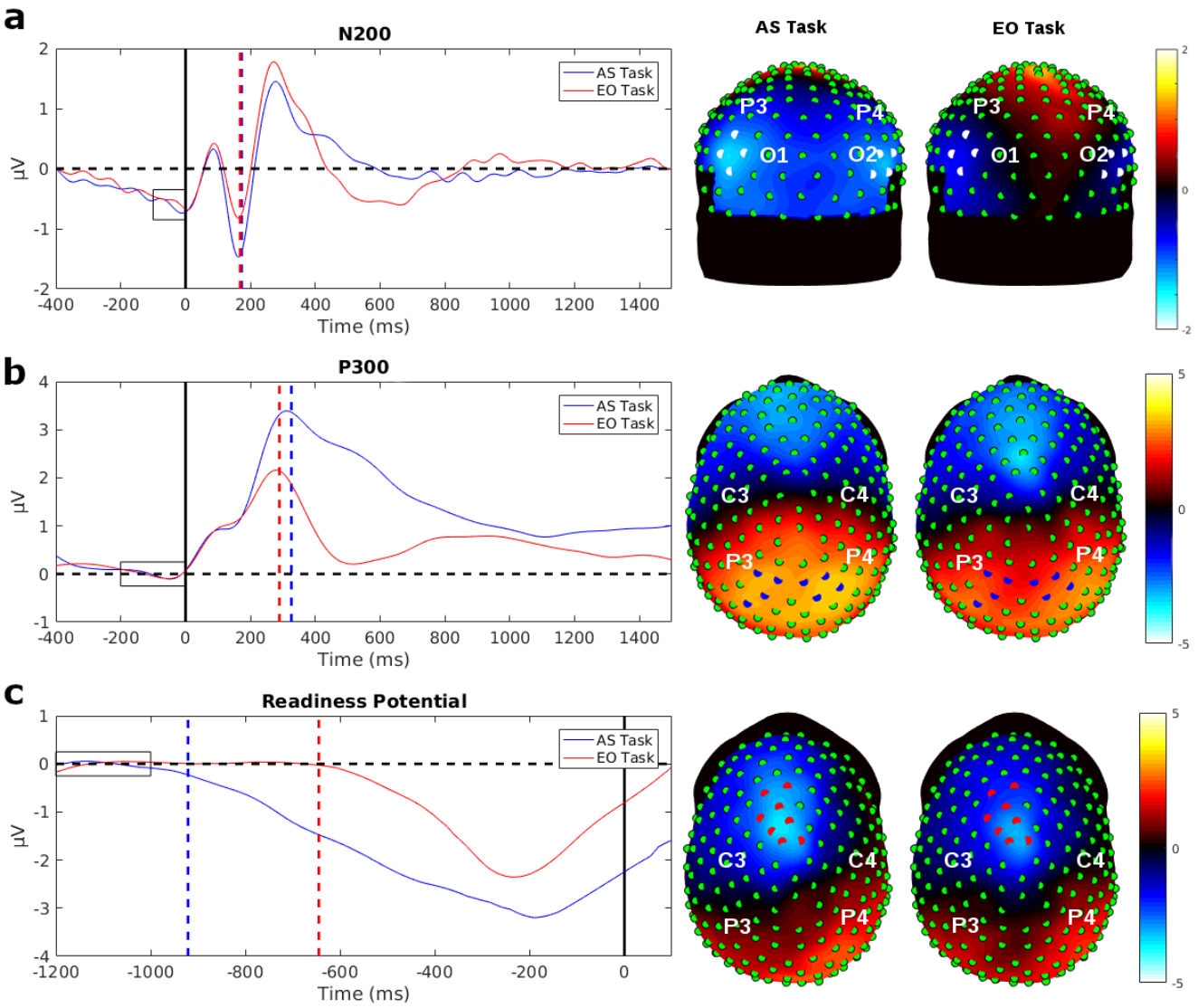

Fig. 3: Evoked potential (EP) waveforms averaged across participants of the 8 strongest electrodes for each EP in the AS task and the EO task. The dashed lines show the median peak latency or median duration time of the signals. The rectangles indicate the baseline interval. On each topographic map the location of these 8 strongest electrodes is indicated and the map show the average potentials in a time window surrounding the peak. a) The N200 waveforms in both of the tasks showed a bilateral distribution over occipital regions in both of the hemispheres. The N200 peak latency was nearly identical between the two tasks. The median N200 peak latency was 173 ms in the AS task and 168.5 ms in the EO task. The topographies show mean potentials of the time interval from 100 ms to 150 ms, where the minimum peak amplitude was for both tasks. b) The P300 waveforms showed a bilateral distribution over parietal cortex for both tasks. The median P300 peak latency for the AS task was 326.5 and 289.5 ms in the EO task, respectively, showing about a 40 ms difference. The topographies show the mean potentials of the time interval from 240 ms to 340 ms, a window covering the peak latency in the two tasks. c) The response-locked RP waveforms showed strongest negativity over the

midline area close to motor areas of the brain. The response-locked RP duration between the tasks varied greatly. The median response-locked RP duration in the AS task was 921 ms and in the EO task was 645 ms. In the AS task, the response-locked RP slowly ramped down to the negative minimum, compared to the EO task where the RP sharply ramped down to the minimum. The EEG topographies represent mean potentials of the time interval from -250 ms to -200 ms, where the minimum peak amplitudes occurred for both tasks.

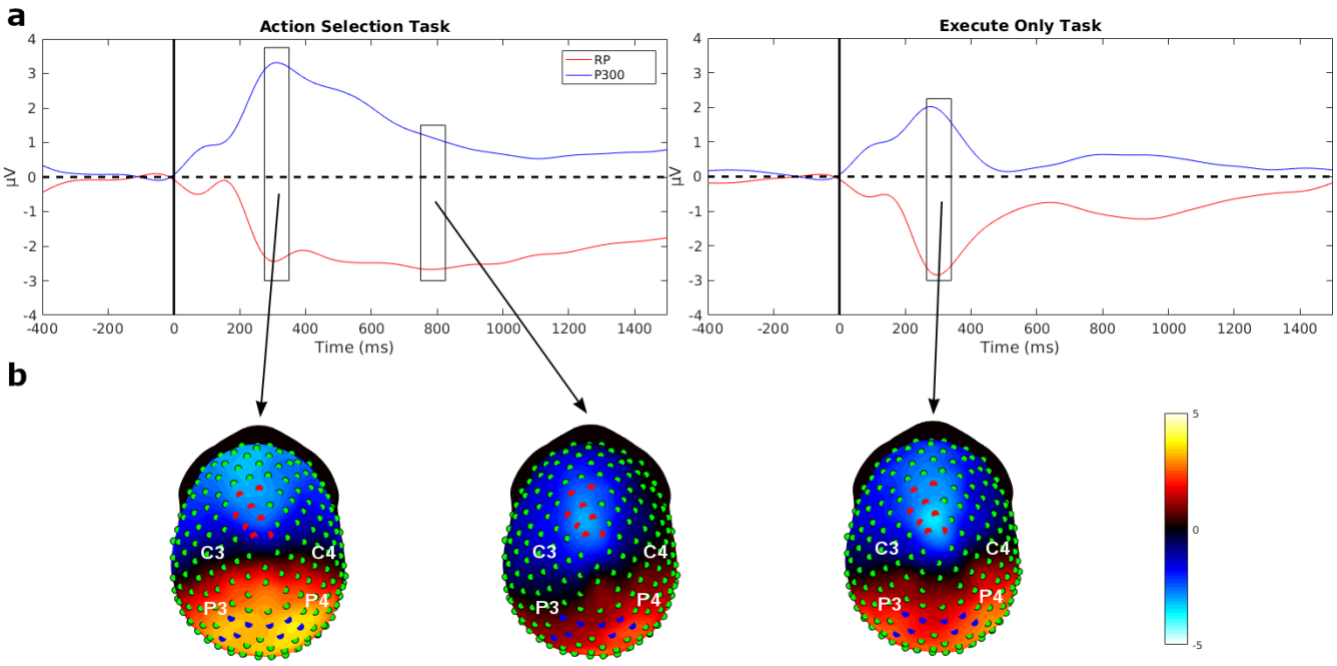

Fig. 4: a) The time series of the stimulus-locked RP and the P300 averaged over the 8 strongest channels. The stimulus-locked RP is shown in the red line, while the P300 is shown by the blue line. The main difference seen between the two tasks are in stimulus-locked RP. In the AS task, after the stimulus-locked RP reached its minimum, there is a sustained negativity, whereas in the EO task, the signal has returned close to baseline. The P300 seemed to display similar time course in both tasks. b) In the AS task, the scalp topography is shown for the average potentials between 300 ms to 350 ms revealing a topography similar to the one seen in Fig. 3b. When a later time period was averaged from 750 ms to 800 ms, the topographic distribution closely corresponded to the response-locked RP (see Fig. 3c). In the EO task, when averaging the potentials around the peak of the two signals, the topography looked similar to the response-locked RP (see Fig. 3c).

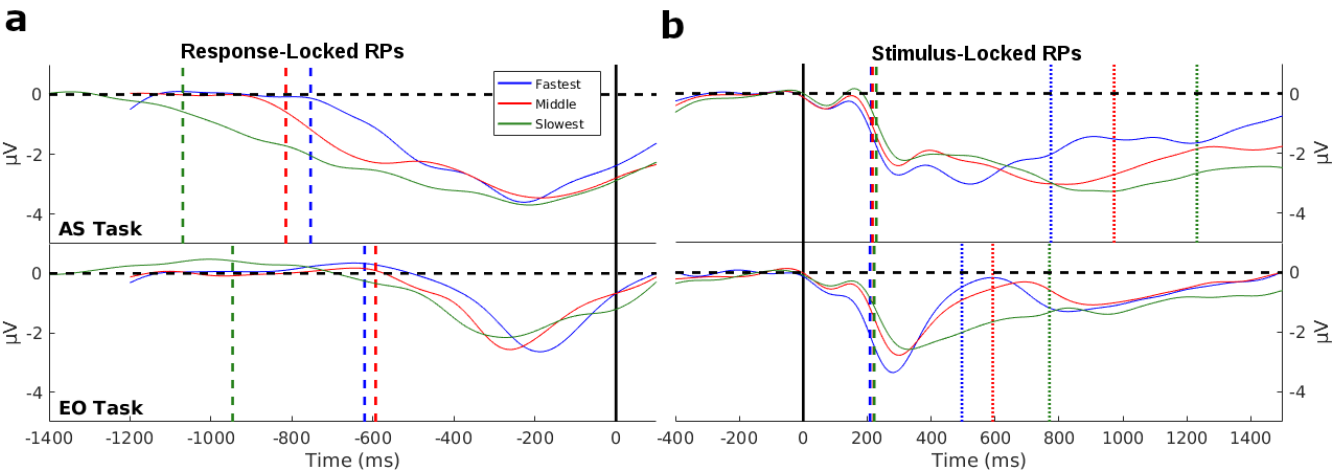

Fig. 5: The RPs of the 8 most negative motor channels averaged together and split into RT tertiles of fastest, middle, and slowest. a) The response-locked RPs for the fastest and middle tertiles are shown for a window of -1200 ms to 100 ms around the response indicated by a black vertical line. For the slowest RT tertile a longer window, -1500 ms to 100 ms around response, was used to accurately estimate response-locked RP duration. The dashed vertical lines represent the response-locked RP duration. In the AS task, the response-locked RP duration varied between conditions revealing the pattern of longer RTs having a longer RP duration. For the EO task, the fastest and middle condition had similar response-locked RP durations, and while the slowest was 300 ms longer. b) The stimulus-locked RPs are shown with a window of -400 ms to 1500 ms around stimulus onset indicated by the black vertical line. The stimulus-locked RP onset times were similar in both tasks for all tertiles as shown by the dashed vertical lines. The dotted vertical lines represent the average RTs in all of the conditions. One subject was excluded from this figure because of very fast RTs compared to the other participants. RP duration and onset times were estimated from this subject and included in the estimates of average duration and onset time and in the regression models shown in Fig. 7.

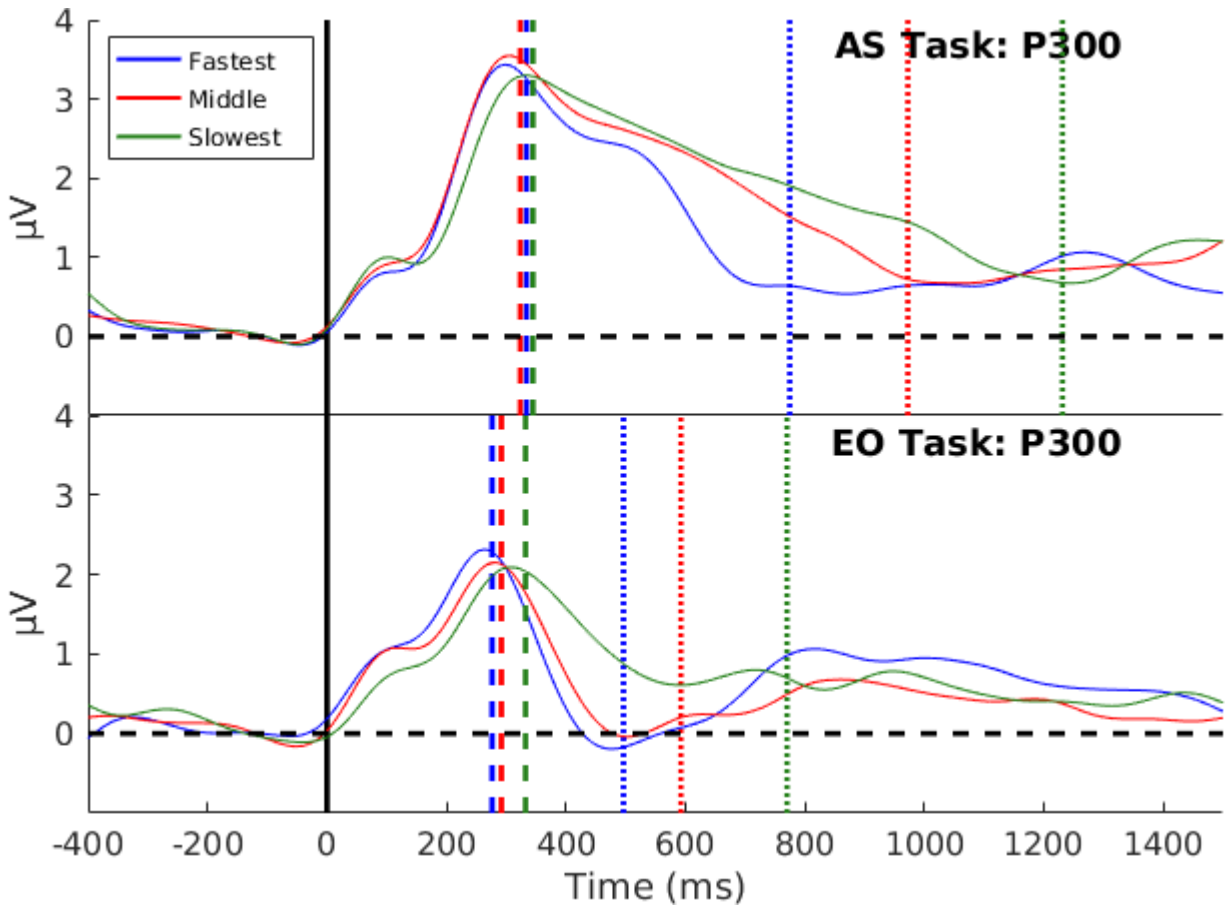

Fig. 6: The P300 signal of the average of the 8 most positive channels over parietal cortex are shown for the data split into RT tertiles in each task. In the AS task, the P300 peak latency is nearly the same in all of the conditions (shown by the vertical dashed line). In the EO task, it was similar in the fastest and middle condition, while the slowest condition showed a delay in peak latency of about 40 ms. This delayed peak in the slowest condition can possibly be due to a lack of attention and arousal during those trials due to the repetitive nature of the EO task. The average RTs for each condition in the two tasks are shown in the vertical dotted lines.

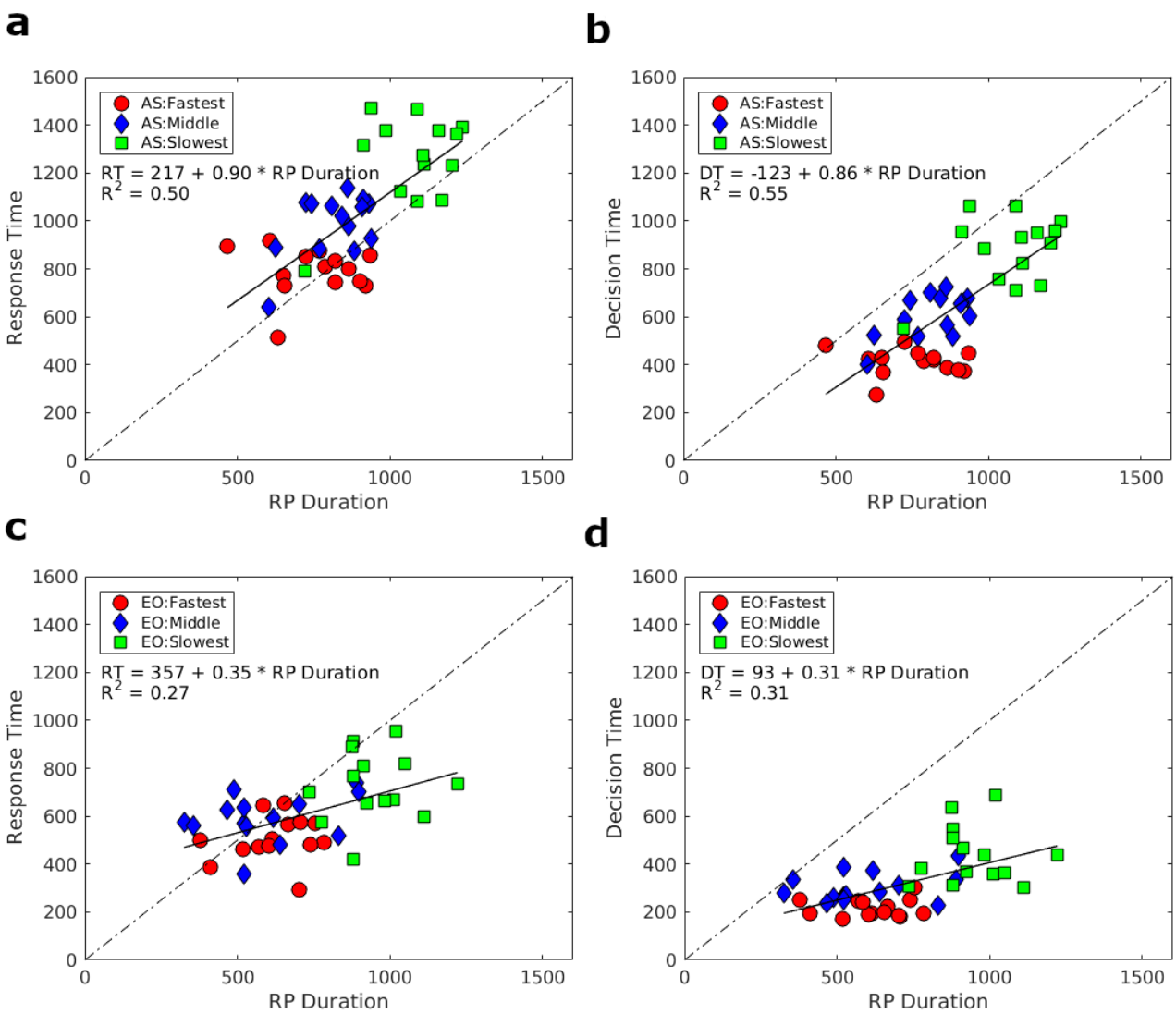

Fig. 7: a) Regression model between response-locked RP duration and median response time for the AS task data divided into RT tertiles. b) Regression model between response-locked RP duration (absolute value of RP onset time) and median decision-making time for the AS task divided into DT tertiles. c) Regression model between response-locked RP duration (absolute value of RP onset time) and median response time for the EO task data divided into RT tertiles. d) Regression model between RP duration (absolute value of RP onset time) and decision-making time for the EO task divided into DT tertiles. For the AS task, RP duration was strongly correlated to both RT and DT, with nearly a one-to-one relationship, indicating that the duration of RP was tracking decision-making process. For the EO task, the correlation was much weaker, and the slope not equal to one.

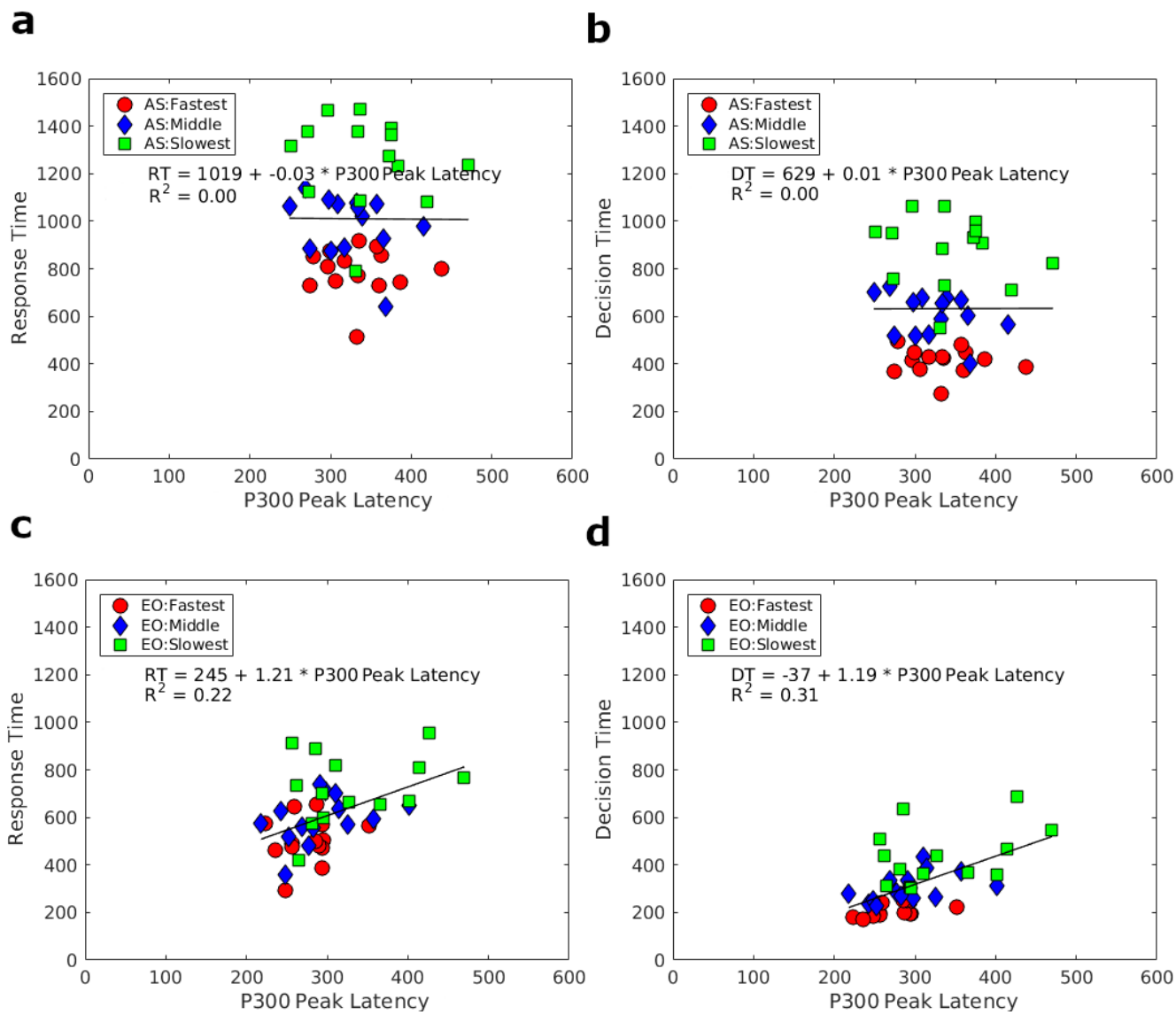

Fig. 8: a) Regression model between P300 peak latency and median response time for the AS task data divided into RT tertiles. b) Regression model between P300 peak latency and median DT for the AS task divided into DT tertiles. c) Regression model between P300 peak latency and median response time for the EO task divided into RT tertiles. d) Regression model between P300 peak latency and DT for the EO task divided into DT tertiles. In the AS task, the P300 peak latency did not significantly correlate with either RT or DT. In the EO task, P300 peak latency was significantly correlated with RT and DT.

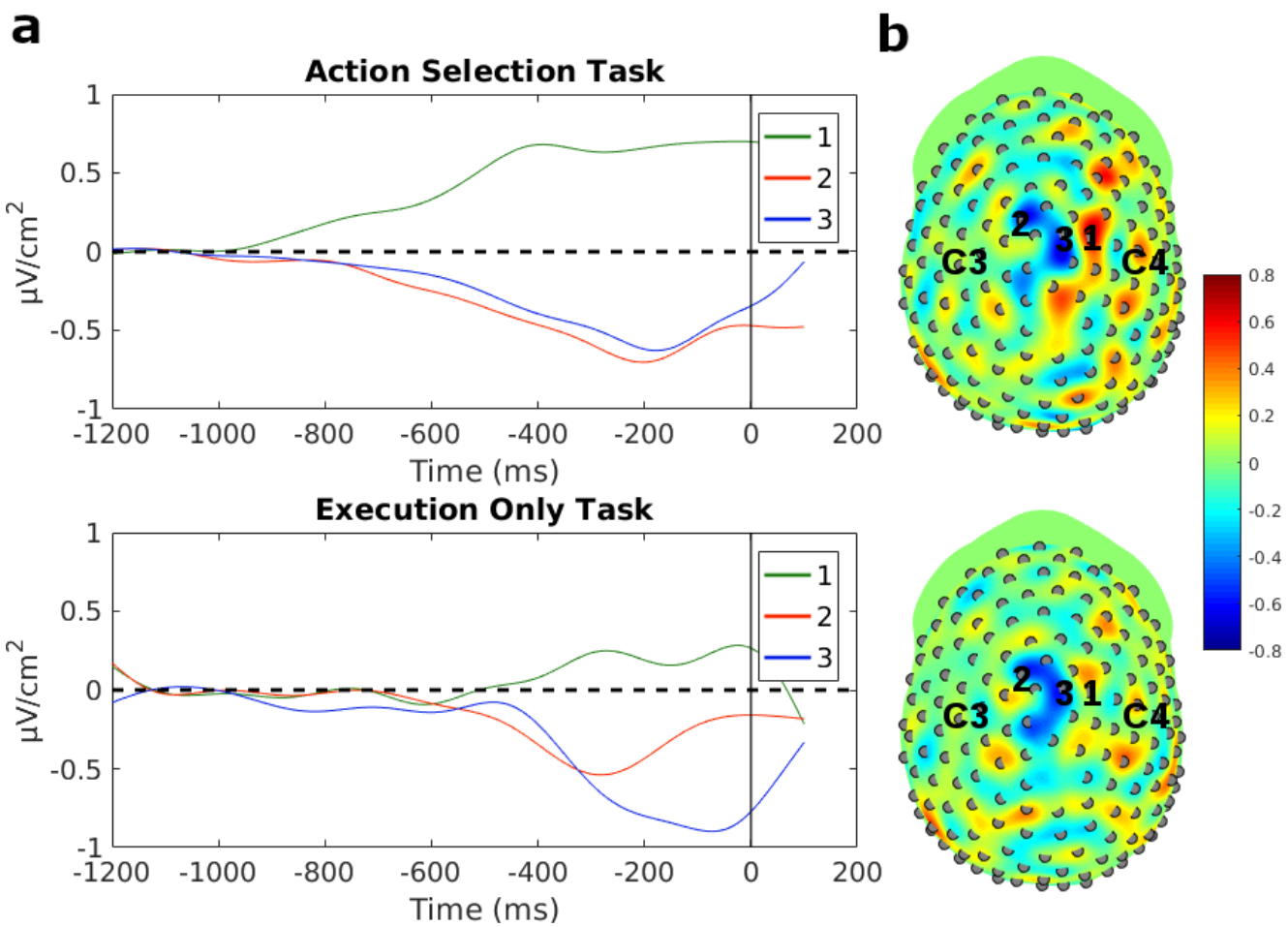

Fig. 9: By applying a surface Laplacian, the strongest current density was localized close to the midline, potentially generated by bilateral structures in the motor cortex close to the midline. There were two electrodes that showed strong negativity over the left midline area and one electrode that showed strong positivity over the right midline area that could be suggestive of lateralization of the motor system. a) The time course of the 3 electrodes that generated the strongest current source density. b) The topography of current source density with the surface Laplacian applied. The three midline electrodes with greatest activity are marked in red, green, and blue and labeled 1-3. For reference, C3 and C4 electrodes are labeled.